Dual-Transducer Malaria Aptasensor Combining Electrochemical Impedance and Surface Plasmon Polariton Detection on Gold Nanohole Arrays

Bohdan Lenyk[+],[a, b] Gabriela Figueroa-Miranda[+],[a, c] Ivan Pavlushko,[a, d] Young Lo,[e] Julian A. Tanner,[e] Andreas Offenhäusser,[a, c] and Dirk Mayer*[a]

Two transducer principles are combined in one aptamer biosensor (aptasensor) by simultaneously performing electrochemical impedance spectroscopy (EIS) and surface plasmon polariton (SPP) detection of a malaria biomarker. A thin gold film perforated with nanohole arrays is modified with small and highly charged aptamer receptors and utilized for the detection of *Plasmodium falciparum* lactate dehydrogenase (PfLDH), the main biomarker of malaria. Monitoring the same analyte binding events by two independent transduction principles not only corroborates the in situ detection, but also covers a concentration range of six orders of magnitude (1 pM–1 μM). The EIS method is highly sensitive to low concentrations of PfLDH (1 pM–100 nM), whereas SPP is sensitive to higher concentrations of the target (10 nM–1 μM), owing to either high interfacial or more bulk sensitivity, respectively. Thus, we propose the dual-transducer aptasensor based on gold nanohole arrays as a platform for a broad dynamic concentration range and reliable detection.

1. Introduction

Recent advances in biotechnology have led to various types of biosensors, widely implemented in the food industry, medicine, biomedical engineering, and environmental applications.[1,2] The performance of the involved transducers tremendously improved, resulting in a high sensitivity permitting even single molecule detection and short analysis times. Moreover, the miniaturization and massive production of biosensors facilitate a low – cost analysis for numerous applications.[3–5] This development is fostered by emerging receptors such as aptamers, which promise low binding constant K_D at low costs and high robustness.

Generally, the optimal operation of every transducer is linked to certain measurement constraints, which limits the accessible concentration interval to the linear dynamic range of detection of the target analyte.[6,7] These constraints are correlated with the intrinsic signal to noise ratio, the penetration depth, and the sensitivity. To overcome the aforementioned limitations and, therefore, to extend the dynamic range of detection, several approaches have been proposed, such as implementing signal amplification strategies, for example, nanomaterials, which increase the number of receptor binding sites, magnify electromagnetic fields, and finally enhance the sensitivity.[8,9] Another way is to perform logical operations by linking different analyte inputs together, which are dependent on each other.[10–12] However, all of these strategies require the usage of several reagents as well as several preparation steps, making the fabrication workflow and operating principle of the biosensor more complicated. Furthermore, the utilization of additional reagents such as nanomaterials increases the risk of malfunctions due to inhomogeneous material properties such as broad size distribution, impurities, degradation, and so on.

Alternatively, a more straightforward approach can be used, where the same receptor system is *in situ* studied by combining different transducer principles.[13] If these transducers possess different dynamic detection ranges then an extension of the latter is achieved. Furthermore, two complementary signals are obtained increasing the reliability of the sensor output. Several types of transducers have been developed for biosensing, including acoustic,[14,15] electrical,[16] optical,[17] and electrochemical[18] methods. The latter two techniques are commonly utilized as Surface Plasmon Resonance (SPR) and Electrochemical Impedance Spectroscopy (EIS) biosensing platforms.

[a] *B. Lenyk,[+] G. Figueroa-Miranda,[+] I. Pavlushko, A. Offenhäusser, Dr. D. Mayer*
Institute of Biological Information Processing (IBI-3)
Forschungszentrum Jülich, 52428 Jülich, Germany
E-mail: dirk.mayer@fz-juelich.de
[b] *B. Lenyk[+]*
Department of Physics
University of Konstanz, 78464 Konstanz, Germany
[c] *G. Figueroa-Miranda,[+] A. Offenhäusser*
RWTH Aachen University
Aachen 52062, Germany
[d] *I. Pavlushko*
Faculty of Radio Physics
Electronics and Computer Systems
Taras Shevchenko National University of Kyiv, Kyiv, 03680, Ukraine
[e] *Y. Lo, J. A. Tanner*
School of Biomedical Sciences
Li Ka Shing Faculty of Medicine
The University of Hong Kong
Pokfulam, Hong Kong Special Administrative Region, China
[+] *These authors contributed equally as the first author to this work*

Supporting information for this article is available on the WWW under https://doi.org/10.1002/celc.202001212

In biomedical diagnostics, EIS has been extensively applied for biosensing, particularly, in antibody and aptamer sensor assays (aptasensors) due to its easy readout, high interface sensitivity, and its label-free detection principle.[19–24] Commonly reported aptasensing impedance measurements are based on Faradaic EIS by implementing redox mediators dissolved in the electrolyte solution. Here, the alteration of the impedance is detected as a response to variations of the analyte concentration and a corresponding blocking of the solution-phase redox species.[22,23,25,26] Noteworthy, whether the impedance signal increases or decreases with rising concentrations depends on the net charge of the analyte in relation to that of the redox probes and can reverse with changing pH values of the medium.

Along with EIS, SPR has been implemented in biosensing applications as a fast, label-free optical method, which exploits evanescent-wave sensing.[27–31] Unlike electrochemical methods, where perturbation of charge distributions caused by the binding of biomarkers to their receptors is detected, SPR techniques translate a change of the refractive index in the vicinity of the surface into an optical signal. The excitation of SPP can be performed by means of prism-coupling,[32] waveguides,[33] and gratings.[34,35]

The combination of the aforementioned methods was previously demonstrated enabling electrokinetic, label-free sensing, enhancing detection accuracy and providing better understanding of biomolecular interactions.[36–42] However, all previous reports utilized antibodies or glycopolymers as receptors, the implementation of a dual transducer biosensor with aptamers as receptor molecules has not been reported so far. Aptamers are small, negatively-charged, single-stranded oligonucleotide sequences, which possess a high binding affinity for their target analytes. Due to their small size, they are extremely confined to the electrode surface, which makes this method highly sensitive to aptamer-target binding events. Such a feature makes aptamers preferred receptor molecules to enhance the sensitivity than big antibody-based receptors.[43–46]

We previously reported the development of an electrochemical aptasensor, using compact gold electrodes for malaria detection by EIS in human serum samples. The detection was achieved through the specific recognition between the 2008s ssDNA aptamer and its target *Plasmodium falciparum* lactate dehydrogenase (PfLDH),[21] a common malaria biomarker. Here we introduce a malaria aptamer-based sensor that combines EIS and SPP detection, where both transducers record *in situ* the same specific binding events between PfLDH and the corresponding 2008s aptamer receptor, which is immobilized to a gold electrode patterned by nanohole arrays (Figure 1). The implementation of a small electro-optical cell together with a portable spectrophotometer facilitates the sensing approach and enables a potential point-of-care application.

A nanohole arrays nicknamed as "holey" gold (hAu) electrodes are optically sensitive not only to binding events happening at the surface,[47–49] but also to physically adsorbed analyte molecules inside the nanoholes and in the bulk medium. Such detection principle can lead to an extended dynamic detection range beyond the limit of the EIS detection restricted more to the surface binding events. Since the PfLDH concentration is directly correlated with the level of parasitemia,[50–52] a broad detection spectrum would be beneficial for the aptasensor implementation not only in the early stages of malaria infection but also along the different stages of the infection as for long-term tracing of drug therapy for detecting possible drug resistance.[53–55]

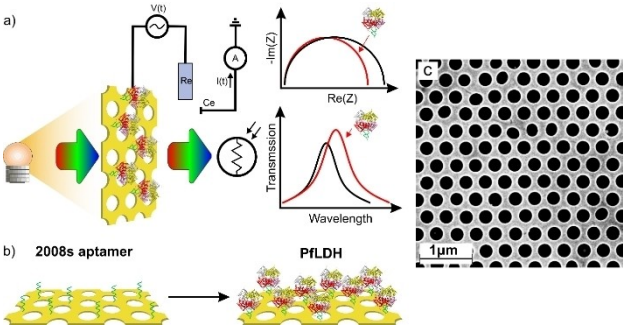

Figure 1. a) Sketch representing the dual aptasensor working principle. EIS and SPP detection are recorded from the gold nanohole array (hAu) electrode synchronously providing Nyquist plots of measured sample impedance and SPP transmission spectra. b) hAu aptasensor with immobilized aptamers and subsequent PfLDH detection. c) SEM image of hAu electrode with a lattice constant of 372 nm and a hole diameter of 245 nm.

2. Results and Discussion

2.1. Electrochemical Impedance Spectroscopy (EIS) Measurements

To fabricate the hAu electrode, we chose a wafer-scale and versatile way by utilizing nanosphere lithography.[56,57] The method relies on the deposition of a monolayer of polystyrene beads onto the surface, reducing the size of the particles by means of Reactive Ion Etching and subsequent metal evaporation on top. The hAu electrodes were fabricated with an average lattice constant of 372 ± 13 nm, a hole diameter of $245\ \text{nm} \pm 15$ nm, and a gold thickness of ~40 nm (Figure 1c). The parameters were chosen not only to take advantage of its high transmission but also to remain sufficient impedance ($50.2 \pm 1.3\ \Omega$) for the electrochemical measurements. Due to the strong absorption of the buffer medium in UV and infrared regions, we aimed to obtain SPP resonances in a transmission window between 500 nm and 900 nm (Supplementary Figure S1).

For our previously reported electrochemical aptasensor, a characteristic change of the impedance signal depending on the pH of the analyte solution was observed.[21] At the physiological pH of 7.5 (commonly working pH), this protein has a positive net-charge due to its isoelectric point (pI = 8.0 for PfLDH). Interestingly, the binding of the positively charged proteins to the small negatively-charged aptamers, which were highly confined to the surface of the electrode, led to an electrostatic attraction of the negatively charged redox probes from the solution phase. Moreover, we demonstrated by

analyzing the aptamer-protein crystal structure that this aptamer binds PfLDH through an extensive salt bridge network, in particularly, through positively charged lysine residues on the protein surface. Therefore, the negative charge of the aptamer backbone is likely to be shielded after binding of the proteins.[58] This combination of electrostatic attraction and shielding effect enhances the charge transfer and leads to a decrement of the measured impedance with increasing protein concentrations.

In this work, the same measurement principle was applied for the hAu electrode. The impedance measured after the immobilization of aptamer, MCH and subsequent PfLDH at different concentrations in a range from 1 pM to 1 μM revealed a decrease of the impedance with increasing protein concentrations (Figure 2). The stepwise impedance aptasensor preparation is documented in detail in Supplementary Figure S2a.

The corresponding electrical equivalent circuit (Inset Figure 2) used for fitting the experimental results contains three main components, namely the solution resistance (R_s), a constant phase element (*CPE*), which represents the imperfect capacitor element due to the intrinsic roughness of the electrode, and the charge transfer resistance (R_{ct}). The last element was used as sensor signal by calculating the percentage change of the charge transfer resistance caused by PfLDH addition. Noteworthy, the impedance measurement obtained for a bare hAu electrode revealed higher resistance of 50 ± 3.4 Ω, compared to a bare compact gold (Au) electrode (5.2 ± 1.3 Ω) (Supplementary Figure S2b). That was expected since the nanoholes reduced the available electrochemically active gold electrode area, which was about 30% smaller for hAu (0.34 cm^2) as compared to a compact Au (0.48 cm^2) electrode with the same geometrical size (defined by the O-ring of the EC-cell). A detailed analysis of the calibration curve obtained by EIS is later discussed in the last section.

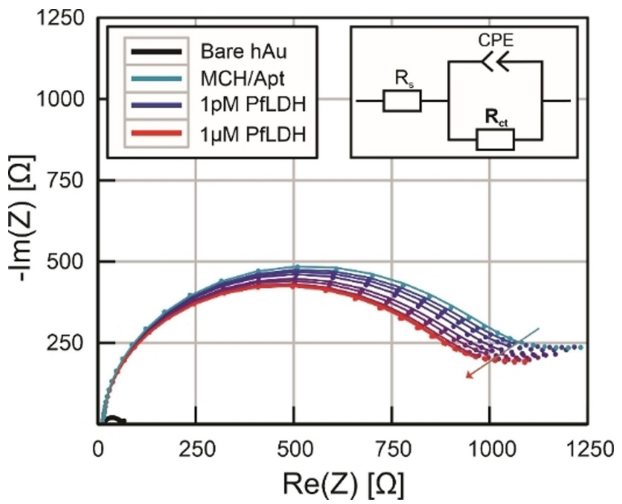

Figure 2. Impedance Nyquist plots obtained for aptamer and MCH immobilization as well as after detection of different concentrations of PfLDH (1 pM–1 μM). The inset depicts the electrical equivalent circuit used to fit the experimental data.

2.2. Surface Plasmon Polariton (SPP) Optical Measurements

Simultaneously with the impedance measurements, the transmission spectrum of hAu electrode was obtained for aptamer and MCH immobilization followed by different PfLDH concentrations. If hAu is considered as a two-dimensional hexagonal assembly of holes, the SPP can be excited for an optically thick metal film by fulfilling the following condition in Equation (1):[59]

$$\vec{k}_{spp} = \vec{k}_{||} + m\vec{G}_x + n\vec{G}_y \quad (1)$$

where $\vec{k}_{spp}$ is the surface plasmon wave vector, $\vec{k}_{||}$ is the incident light component of the wave vector parallel to the surface, $\vec{G}$ is the reciprocal vector of the grating lattice, and *m* and *n* are integers. Taking the perpendicular incident light and the hexagonal array lattice into account, the position of SPP resonance can be estimated by Equation (2):[60]

$$\lambda_{spp} = \frac{d}{\sqrt{\frac{4}{3}(m^2 + mn + n^2)}} \sqrt{\frac{\varepsilon(\omega)_m \varepsilon_d}{\varepsilon(\omega)_m + \varepsilon_d}} \quad (2)$$

where *d* is lattice constant, $\varepsilon(\omega)_m$, and ε_d are the dielectric constants of the metal and the dielectric substrate, respectively. Using the values of the gold dielectric function[61] and the dielectric constant of the quartz substrate $\varepsilon_d = 2.25$, the position of SPP resonance is anticipated to be positioned at around 580 nm for (m, n) = (1, 0) and a lattice constant of 372 nm. However, we observed the SPP peak at around 720 nm (Figure 3a, black curve), which is in a noticeable disagreement with the calculated value and can be explained by the effect of an optically thin film and additional adhesive titanium layer.[62,63]

The change of the refractive index (RI) of the medium caused by adding buffer solution led to a redshift of transmission resonance from ~720 nm to ~788 nm. Moreover, the overall transmission at SPP resonance increased by around 10%, originated from waveguided light inside the nanoholes.[64] Furthermore, the redshift continued from 788.4 nm to 793.2 nm after immobilization of aptamer and MCH, and subsequent detection of different concentrations of PfLDH. To determine the positions of the resonances, the transmission curves were fit with a Fano resonance function[63] (Figure 3a, inset). The hAu electrode exhibited a relatively low Q factor of 1.9, which can be increased to improve the resolution of detection by varying hole diameter and Au thickness, if required (Supplementary Figure S3). Furthermore, the PfLDH concentrations starting from 50 nM to higher caused a uniform and gradual decrement of transmittance at the SPP resonance. This is likely to be associated with the high concentration of molecules, which made the medium more optically dense.

To corroborate the experimental optical findings, we performed FDTD simulations modelling the hAu electrode with the aptamer/protein complex layer (Figure 3b, Supplementary Figure S4). The formation of a 2008s aptamer film with 100% coverage of all PfLDH adsorption sites was simulated as a thin dielectric layer with a thickness of 8 nm[58] and a refractive index of 1.42.[65,66] We assumed that the layer completely covers the

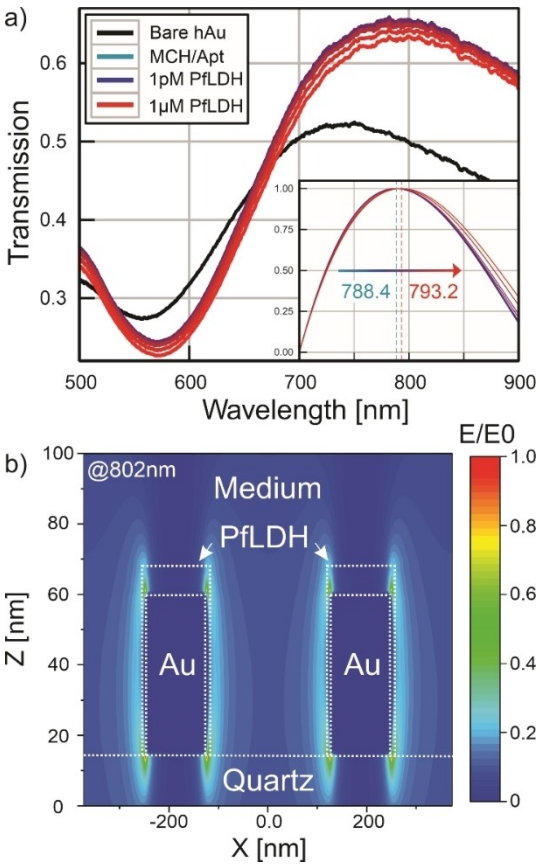

Figure 3. a) Transmission spectra of a bare gold nanohole arrays in air (black) and with different concentrations of PfLDH (1 pM–1 µM) (blue-red) in buffer medium solution. The inset shows the zoom of normalized and fit transmission spectra at the surface plasmon polariton resonance revealing a red peak shift from 788.4 nm to 793.2 nm. b) FDTD simulated electrical field in the *x-z* cross-section of hAu electrode in the buffer medium.

gold surface, including the walls of the nanoholes. The 2D cross section revealed the distribution of the surface confined electrical field gradually decaying from the edges of the nanoholes into the bulk medium. This indicates that not only the aptamer/protein complex is detected by SPP, but also physically absorbed molecules inside the nanoholes contribute to the change of effective RI within the electrical field, which, therefore, adds the redshift of the SPP resonance.

2.3. EIS & SPP Calibration Curves

Generally, a calibration curve shows the response of the detection method by changes in the concentration of the target analyte. In this way, it helps to determine the concentration of the target in an unknown sample. From such plot, the limit of detection (LOD), which represents the lowest confidence detection value as well as the sensitivity (S) from the linear dynamic response can be obtained. The LOD of the aptasensor was determined according to the formula: $LOD = 3 \times \sigma_0$, where σ_0 represents the standard deviation of the blank substrate.[67] Here, we plotted together the calibration curves obtained from EIS and SPP measurements performed in parallel in the electrochemical/optical flow cell (Figure 4). The detection range of each transducer was fit to the Langmuir-Freundlich adsorption isotherm (Eq. 3),[68] which provides a simple model to describe the adsorption mechanism of the system quantitatively and can be utilized to estimate a protein binding affinity.

$$\theta = \frac{K_{eq} \cdot c^n}{1 + K_{eq} \cdot c^n} \tag{3}$$

where θ stands for coverage, K_{eq} is the equilibrium constant, c is the protein concentration, and n is the homogeneity coefficient with a value from 0 to 1. Since the coverage θ is linearly proportional to the signal change, we can modify the formula in order to apply it to both EIS and SPP experimental data. This linear proportionality has some limitations, in particular for EIS due to the unspecific adsorption and voltage perturbation[69] (See Supporting Information).

The implementation of the formula in the impedance measurements results in Equation (4):

$$\frac{\Delta R_{ct}}{R_{ct0}} = \frac{\left(\frac{\Delta R_{ct}}{R_{ct0}}\right)_{max} \cdot K_{eq} \cdot c^n}{1 + K_{eq} \cdot c^n} \tag{4}$$

where R_{ct0} stands for the charge transfer resistance before and ΔR_{ct} for the change of the transfer resistance after protein binding. The obtained calibration curve (Figure 4, blue line) revealed a broad linear range in the semi-logarithmic scale from 1 pM to 100 nM before reaching saturation at 1 µM (~20%). A low extracted LOD was obtained with a value of 1.4 pM and a sensitivity of 2.7 ± 0.16/decade. The hAu electrode revealed a similar PfLDH limit of detection compared with impedance data obtained by using compact gold (Au) electrodes (LOD = 2 pM, Figure S5). Besides, the upper limit of detection range was expanded for the hAu electrode by 2 orders of magnitude. The hAu exhibited the maximum detected concentration at around 100 nM before reaching the steady saturation range, which in the case of the compact Au electrode was already reached at a

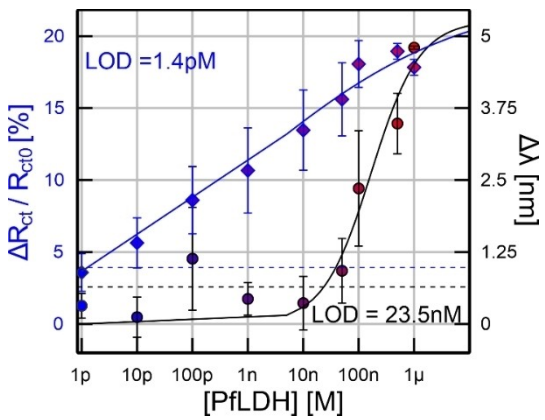

Figure 4. Calibration curves obtained for PfLDH detection by simultaneously performed EIS (blue) and SPP (black) measurements with the hAu-based electrode aptasensor.

lower concentration of 1 nM. Furthermore, the SPP measurements extended the upper detection limit by 2 other orders of magnitude more. The experimental data were fit with the following Equation (5):

$$\Delta\lambda = \frac{\Delta\lambda_{max} \cdot K_{eq} \cdot c^n}{1 + K_{eq} \cdot c^n} \quad (5)$$

where $\triangle\lambda$ is the SPP shift. Unlike EIS, the calibration curve showed a response smaller than the LOD signal for low concentrations of PfLDH ($<$ 1nM) and exhibited a linear relation in the semi-logarithmic presentation for concentrations of up to 1 μM without reaching saturation. Fitting of the experimental data suggests an extension of the detection range to 10 μM. The extracted LOD and sensitivity were 23.5 nM and 2.21 $\pm$ 0.31/decade, respectively.

Because of such specific geometry created by the nanoholes, we assume that both EIS and SPP detected physically absorbed proteins that could form adlayers inside the nanoholes, which led to the extension of the detection range. The evanescent field of the SPP decays further into the analyte medium and is, therefore, able to detect larger number of molecules. Moreover, the detection range may be increased even further due to the high bulk sensitivity, similarly as previously reported.[37,38] In the case of the EIS, since this method is sensitive to surface binding but not to bulk changes, the possible formation of adlayers, beyond the actual aptamer-protein complex might also explain the signal enhancement. The higher amount of positively-charged proteins inside the nanoholes enhances the attraction of more negatively redox probes, which leads to the further decrease of charge transfer resistance, and expanding in this way the concentration of detected analyte as compared with the compact gold electrode. For the PfLDH detection, the dual EIS/SPP aptasensor has helped to obtain a broad dynamic detection range of 6 orders of magnitude. Therefore, the combination of these two label-free methods is of great advantage for protein analyte *in situ* detection as a discriminatory tool of false positive results.

Additionally, we investigated the selectivity of the hAu aptasensor, by performing dual EIS and SPP detection of human LDHB (hLDHB), an analogue protein of PfLDH. The specific selectivity of the 2008s aptamer for PfLDH versus human LDH was already established during the SELEX process by a counter target selection of the aptamer.[58] Both EIS and SPP methods revealed simultaneous lower unspecific detection for hLDHB as compared with the target PfLDH (Supplementary Figure S6). A slightly higher unspecificity detected by SPP measurements might be related, as discussed above, with the bulk sensitivity of protein present in the medium that changes its RI but not with unspecific detection by the aptamer. The selectivity was proven with medium (50 nM) and high (500 nM) concentration of both proteins.

3. Conclusions

We established an aptamer-modified biosensor based on hAu electrodes, by combining SPP and EIS methods for the *in situ* detection of PfLDH. The combination of both methods enabled sensitive detection of PfLDH at low concentrations, achieved mainly by impedance measurements. On the other hand, the implementation of an optical method helped, apart from corroborating at the same time the detection, to expand the overall dynamic detection range to six orders of magnitude with the highest PfLDH concentration tested (1 μM). The upper limit of detection is expected to be extended even further, since a saturation of the optical signal was not yet observed.

Furthermore, we were able to investigate by means of the FDTD simulation the origins of the difference between electrochemical and optical results, regarding detection limit and expanded dynamic detection range. The simulation confirmed that due to the long decay length of the electrical field (around 30 nm), the SPP detection enables to sense not only PfLDH bound to aptamers, but also protein adlayers assembled inside the nanoholes within the decay length. Such an extra assembled protein layer also explains the improved PfLDH detection by EIS with the hAu electrode as compared with compact Au electrode. Aforementioned findings are beneficial for the aptasensor implementation as a long-term detection method for possible drug resistance tracking on patients.

Experimental Section

Reagents

Malaria 2008s aptamer (5'-HO–$(CH_2)_6$–S–S–$(CH_2)_6$–O– CTG GGC GGT AGA ACC ATA GTG ACC CAG CCG TCT AC-3') was synthesized by Friz Biochem GmbH (Neuried, Germany). The recombinant Plasmodium falciparum lactate dehydrogenase (PfLDH) and human lactate dehydrogenase B (hLDHB) were obtained from bacterial expression[58] 25 mM Tris-HCl buffer (NaCl 0.1 M, Tris 25 mM, HCl 25 mM, pH 7.5) and high salt concentration phosphate-buffered saline (PBS, 10 mM sodium phosphate with 1.0 M NaCl and 1 mM Mg^{2+}, pH 7.5) were prepared. Tris (2-carboxyethyl) phosphine hydrochloride (TCEP), 6-mercapto-1-hexanol (6-MCH), potassium ferricyanide ($K_3[Fe(CN)_6]$), potassium ferrocyanide ($K_4[Fe(CN)_6]$) trihydrate, acetone, isopropanol, and ethanol were purchased from Merck/Sigma-Aldrich Chemie GmbH (Darmstadt, Germany). All aqueous solutions were prepared using Milli-Q ultra-pure deionized water (18.2 MΩ cm, Millipore, Merck, Darmstadt, Germany).

Fabrication of hAu Electrode

To fabricate hAu electrode, we utilized the nanosphere lithography, where particles were deposited by means of the funnel-assisted interfacial assembly technique.[70] The 4″ quartz substrate (Plan Optik AG, Germany) was cleaned in acetone, and isopropanol followed by oxygen plasma treatment at 0.7 mbar with 200 W for 5 min. The substrate was then placed within a plastic funnel inside a beaker filled with Milli-Q water. To provide a good transition from solution into the interface and improve packing of the particle layer, a small amount of aqueous solution of 10 mM Triton-X 100 was added in Milli-Q water resulting in around 10 nM concentration. A polystyrene (PS) particle dispersion of 382 nm diameter

with low functionalization (Bang Laboratories, USA) (5%) was mixed with ethanol in a 1:1 ratio. The particle solution was gradually assembled onto the water-air interface resulting in a monolayer of PS particles covering the entire surface. The PS monolayer then was transferred onto the substrate by pumping out water, while the plastic funnel supported the packing during deposition.

The reduction of the particle size was made by utilizing Reactive Ion Etching (RIE, Oxford Instruments, Great Britain) using a combination of O_2 and CHF_3 in a ratio of 40:10 sccm. The etching process was performed at 0.026 mbar, 0 °C, and radiofrequency power (RF) of 30 W for 4 min. The subsequent metallization step was conducted by e-beam evaporation of 5 nm Ti and 40 nm Au at a deposition rate of 0.1 nm/sec and 0.5 nm/sec, respectively. The particle lift-off was done by adhesive cello - tape followed by sonication in acetone. In order to fit the dimensions of the electrochemical/optical flow cell chamber, the 4'' wafer was diced to 25×25 mm^2 samples.

Scanning Electron Microscopy (SEM) was utilized to obtain high-resolution images of hAu electrode. We used Zeiss Gemini 1550 system (Zeiss, Germany) employing an in-lens detector with 10 kV applied acceleration voltage.

Stepwise hAu Aptasensor Preparation

The hAu chip was sonicated for 5 min in acetone followed by another 5 min in isopropanol, subsequently rinsed with Milli-Q water and dried with N_2 flow. Finally, it was cleaned by O_2 plasma treatment for 3 min with a pressure of 0.5 mbar and power of 100 W, followed by placing it in ethanol for 30 min to achieve the Au oxide reduction.

Immediately after the cleaning procedure the hAu chip was mounted in the previously cleaned electrochemical/optical flow cell. A volume of 4 mL 25 mM Tris-HCl buffer followed by 4 mL of Milli-Q water were always flushed with maximum flow rate ($\approx$8 mL/min) before addition of the aptamer. The activation of the aptamer was executed by incubating it with 10 mM TCEP solution for 1 h. This step was done to split the disulfide-protecting bond, thus, permitting the immobilization of the aptamer on the hAu surface. In the subsequent step, 0.5 μM of the early activated 2008s aptamer was resuspended in 10 mM high salt PBS buffer solution and the solution left circulating overnight with a continuous flow rate. Unless otherwise stated, the flow rate was controlled to 70 μL/min for all the subsequent steps using a peristaltic pump (Reglo Digital ISM596, Cole-Parmer, Germany). After the overnight incubation time, the cell was rinsed, to remove non-chemically bound aptamers, by flowing 4 mL of 25 mM Tris-HCl buffer and 4 mL of Milli-Q. Then, the sensor was left in continuous flow with 1 mM mercapto-hexanol in ethanol solution for 1 hour to block the free receptor spaces and to orient the immobilized ssDNA aptamer upwards forming a compact monolayer. After the blocking time, it was rinsed with a flow of ethanol, Tris-HCl buffer and Milli-Q to also flush away all non-covalently bound molecules. Once the aptasensor was ready, the optical and electrochemical measurements were performed simultaneously before and after incubation with the corresponding PfLDH concentration in 25 mM Tri-HCl buffer with 5 mM $[Fe(CN)_6]^{3-/4-}$ solution. For PfLDH detection, after lapsed 15 min of continuous flow, it was stopped for performing the measurements.

Dual Impedance/Optical Measurements

The dual EIS and SPP detection experiments were conducted by employing a spectroelectrochemical flow cell (redoxme AB, Sweden), which was designed and modified to perform simultaneous electrochemical (impedance) and (transmission) optical measurements. It consists of a polyether ether ketone flow chamber equipped with a magnetic mount sample holder for the hAu electrode with the size of 25×25 mm^2. The total internal volume of the chamber is 0.7 mL, which allows to shorten the optical path to 4 mm and, therefore, reduces the absorption of output light. The cell is equipped with two collimating lenses for input and output light, which provides parallel irradiation of the sample. In addition, SMA 905 connectors are applied to facilitate the optical fiber connection. The cell also has adequate electrode plugs for pseudo-reference and counter platinum (Pt) electrodes.

The impedance spectroscopy and optical transmittance characterizations were performed at least three times in 25 mM Tri-HCl buffer with 5 mM $[Fe(CN)_6]^{3-/4-}$ at pH 7.5. The EIS measurements were performed by employing a VSP-300 potentiostat (Biologic Science Instruments, France) of three-electrode system, using the provided platinum wire as the counter electrode (CE), a pseudo-reference platinum wire as the reference electrode (RE), and the hAu electrode with the immobilized aptamer/MCH monolayer as the working electrode (WE). The EIS measurements were recorded at a set potential of 0 V in accordance with the CV results using a pseudo-reference platinum electrode since this is the redox potential of the $[Fe(CN)_6]^{3-/4-}$ redox probe. The frequency range used was from 10 kHz to 1 Hz with an amplitude of 0.01 V.

A mobile spectrometer CCS200/M (Thorlabs, USA) was used in combination with a QTH10(/M) quartz-tungsten-halogen lamp (Thorlabs, USA) for optical measurements. The lamp was equipped with lenses that were adjusted in order to collimate the light into an optical fiber that was connected to the input SMA 905 connector, while the output connector was attached directly to the spectrometer. The measuring parameters including integration time were adjusted to get the smallest signal to noise ratio.

Finite Difference Time Domain (FDTD) Simulation

The simulation of the transmission spectrum and electrical field distribution of hAu electrodes covered with aptamer-protein layer was performed by using FDTD package from Lumerical Inc. (Vancouver, Canada). The models for quartz, Ti and Au were taken from default database, the model for aptamer-protein layer was chosen as a dielectric with RI of 1.42. The source of light was applied along the z-axis perpendicularly to the substrate surface. The symmetric/antisymmetric boundary conditions were applied with x and y meshing of 3 nm and z meshing of 1 nm.

Acknowledgements

The work was supported by a grant from the German Research Foundation (DFG), funding code MA 2151/3-1, the Mexican National Council for Science and Technology (CONACyT) and the German Academic Exchange Service (DAAD) with the grant number 448904. Open access funding enabled and organized by Projekt DEAL.

Conflict of Interest

The authors declare no conflict of interest.

Keywords: electrochemistry · surface plasmon resonance · malaria detection · aptamers · electro-optical devices

[1] C. M. Pandey, B. D. Malhotra, *Biosensors*, De Gruyter, Berlin, Boston **2019**.
[2] S. Kara, Ed., *A Roadmap of Biomedical Engineers and Milestones*, InTech **2012**.
[3] B. R. Goldsmith, L. Locascio, Y. Gao, M. Lerner, A. Walker, J. Lerner, J. Kyaw, A. Shue, S. Afsahi, D. Pan, J. Nokes, F. Barron, *Sci. Rep.* **2019**, *9*, 434.
[4] E.-H. Yoo, S.-Y. Lee, *Sensors* **2010**, *10*, 4558–4576.
[5] B. D. Malhotra, A. Chaubey, *Sens. Actuators B* **2003**, *91*, 117–127.
[6] P. Mehrotra, *J. Oral Biol. Craniofacial Res.* **2016**, *6*, 153–159.
[7] S. Vigneshvar, C. C. Sudhakumari, B. Senthilkumaran, H. Prakash, *Front. Bioeng. Biotechnol.* **2016**, *4*, 11.
[8] A. Bonanni, M. del Valle, *Anal. Chim. Acta* **2010**, *678*, 7–17.
[9] Q. Chen, W. Tang, D. Wang, X. Wu, N. Li, F. Liu, *Biosens. Bioelectron.* **2010**, *26*, 575–579.
[10] L. Feng, Z. Lyu, A. Offenhäusser, D. Mayer, *Angew. Chem. Int. Ed.* **2015**, *54*, 7693–7697; *Angew. Chem.* **2015**, *127*, 7803–7808.
[11] Z. Li, M. A. Rosenbaum, A. Venkataraman, T. K. Tam, E. Katz, L. T. Angenent, *Chem. Commun.* **2011**, *47*, 3060.
[12] F. Xia, X. Zuo, R. Yang, R. J. White, Y. Xiao, D. Kang, X. Gong, A. A. Lubin, A. Vallée-Bélisle, J. D. Yuen, B. Y. B. Hsu, K. W. Plaxco, *J. Am. Chem. Soc.* **2010**, *132*, 8557–8559.
[13] A. Y. Zhu, F. Yi, J. C. Reed, H. Zhu, E. Cubukcu, *Nano Lett.* **2014**, *14*, 5641–5649.
[14] R. Fogel, J. Limson, A. A. Seshia, *Essays Biochem.* **2016**, *60*, 101–110.
[15] N. G. Durmuş, R. L. Lin, M. Kozberg, D. Dermici, A. Khademhosseini, U. Demirci, *Encycl. Microfluid. Nanofluidics*, Springer New York, New York, NY **2015**, pp. 28–40.
[16] X. Luo, J. J. Davis, *Chem. Soc. Rev.* **2013**, *42*, 5944–5962.
[17] C. Chen, J. Wang, *Analyst* **2020**, *145*, 1605–1628.
[18] B.-Y. Chang, S.-M. Park, *Annu. Rev. Anal. Chem (Palo Alto, Calif.)* **2010**, *3*, 207–229.
[19] D. Zhang, Y. Lu, Q. Zhang, L. Liu, S. Li, Y. Yao, J. Jiang, G. L. Liu, Q. Liu, *Sens. Actuators B* **2016**, *222*, 994–1002.
[20] X. Li, L. Shen, D. Zhang, H. Qi, Q. Gao, F. Ma, C. Zhang, *Biosens. Bioelectron.* **2008**, *23*, 1624–1630.
[21] G. Figueroa-Miranda, L. Feng, S. C.-C. Shiu, R. M. Dirkzwager, Y.-W. Cheung, J. A. Tanner, M. J. Schöning, A. Offenhäusser, D. Mayer, *Sens. Actuators B* **2018**, *255*, 235–243.
[22] Y. Zhang, G. Figueroa-Miranda, Z. Lyu, C. Zafiu, D. Willbold, A. Offenhäusser, D. Mayer, *Sens. Actuators B* **2019**, *288*, 535–542.
[23] S. Lee, K.-M. Song, W. Jeon, H. Jo, Y.-B. Shim, C. Ban, *Biosens. Bioelectron.* **2012**, *35*, 291–296.
[24] T. Bertok, L. Lorencova, E. Chocholova, E. Jane, A. Vikartovska, P. Kasak, J. Tkac, *ChemElectroChem* **2019**, *6*, 989–1003.
[25] D. Pihikova, P. Kasak, P. Kubanikova, R. Sokol, J. Tkac, *Anal. Chim. Acta* **2016**, *934*, 72–79.
[26] L. Chen, Z.-N. Chen, *Talanta* **2015**, *132*, 664–668.
[27] X. Fan, I. M. White, S. I. Shopova, H. Zhu, J. D. Suter, Y. Sun, *Anal. Chim. Acta* **2008**, *620*, 8–26.
[28] A. G. Brolo, *Nat. Photonics* **2012**, *6*, 709–713.
[29] J. Homola, *Chem. Rev.* **2008**, *108*, 462–493.
[30] J. R. Mejía-Salazar, O. N. Oliveira, *Chem. Rev.* **2018**, *118*, 10617–10625.
[31] E. Mauriz, P. Dey, L. M. Lechuga, *Analyst* **2019**, *144*, 7105–7129.
[32] K. Matsubara, S. Kawata, S. Minami, *Appl. Opt.* **1988**, *27*, 1160.
[33] L. Wu, J. Guo, H. Xu, X. Dai, Y. Xiang, *Photonics Res.* **2016**, *4*, 262.
[34] S. Rossi, E. Gazzola, P. Capaldo, G. Borile, F. Romanato, *Sensors* **2018**, *18*, 1621.
[35] B. Lenyk, V. Schöps, J. Boneberg, M. Kabdulov, T. Huhn, E. Scheer, A. Offenhäusser, D. Mayer, *Nano Lett.* **2020**, *20*, 5243–5250.
[36] S. Boussaad, J. Pean, N. J. Tao, *Anal. Chem.* **2000**, *72*, 222–226.
[37] J. Lu, W. Wang, S. Wang, X. Shan, J. Li, N. Tao, *Anal. Chem.* **2012**, *84*, 327–333.
[38] S. Patskovsky, V. Latendresse, A.-M. Dallaire, L. Doré-Mathieu, M. Meunier, *Analyst* **2014**, *139*, 596–602.
[39] J. Lazar, R. R. Rosencrantz, L. Elling, U. Schnakenberg, *Anal. Chem.* **2016**, *88*, 9590–9596.
[40] J. Juan-Colás, S. Johnson, T. F. Krauss, *Sensors* **2017**, *17*, 1–15.
[41] J. A. Ribeiro, M. G. F. Sales, C. M. Pereira, *Sens. Actuators B* **2020**, *316*, 128129.
[42] P. Aspermair, U. Ramach, C. Reiner-Rozman, S. Fossati, B. Lechner, S. E. Moya, O. Azzaroni, J. Dostalek, S. Szunerits, W. Knoll, J. Bintinger, *J. Am. Chem. Soc.* **2020**, *142*, 11709–11716.
[43] S. Song, L. Wang, J. Li, C. Fan, J. Zhao, *TrAC Trends Anal. Chem.* **2008**, *27*, 108–117.
[44] A. E. G. Cass, Y. Zhang, *Faraday Discuss.* **2011**, *149*, 49–61.
[45] T. Hianik, J. Wang, *Electroanalysis* **2009**, *21*, 1223–1235.
[46] G. Figueroa-Miranda, C. Wu, Y. Zhang, L. Nörbel, Y. Lo, J. A. Tanner, L. Elling, A. Offenhäusser, D. Mayer, *Bioelectrochemistry* **2020**, *136*, 107589.
[47] C. Escobedo, *Lab Chip* **2013**, *13*, 2445–2463.
[48] A. Prasad, J. Choi, Z. Jia, S. Park, M. R. Gartia, *Biosens. Bioelectron.* **2019**, *130*, 185–203.
[49] J. Jiang, X. Wang, S. Li, F. Ding, N. Li, S. Meng, R. Li, J. Qi, Q. Liu, G. L. Liu, *Nat. Photonics* **2018**, *7*, 1517–1531.
[50] A. Moody, *Clin. Microbiol. Rev.* **2002**, *15*, 66–78.
[51] S. K. Martin, G.-H. Rajasekariah, G. Awinda, J. Waitumbi, C. Kifude, *Am. J. Trop. Med. Hyg.* **2009**, *80*, 516–22.
[52] R. Piper, J. Lebras, L. Wentworth, A. Hunt-Cooke, S. Houzé, P. Chiodini, M. Makler, *Am. J. Trop. Med. Hyg.* **1999**, *60*, 109–18.
[53] S. Houzé, L. Wentworth, P. Chiodini, A. Hunt-Cooke, R. Piper, M. Makler, J. Lebras, *Am. J. Trop. Med. Hyg.* **1999**, *60*, 109–118.
[54] J. Waitumbi, G. Awinda, G.-H. Rajasekariah, C. Kifude, S. K. Martin, *Am. J. Trop. Med. Hyg.* **2009**, *80*, 516–522.
[55] R. M. Dirkzwager, A. B. Kinghorn, J. S. Richards, J. A. Tanner, *Chem. Commun.* **2015**, *51*, 4697–4700.
[56] B. Ai, Y. Yu, H. Möhwald, G. Zhang, B. Yang, *Adv. Colloid Interface Sci.* **2014**, *206*, 5–16.
[57] Y. Wang, M. Zhang, Y. Lai, L. Chi, *Nano Today* **2018**, *22*, 36–61.
[58] Y.-W. Cheung, J. Kwok, A. W. L. Law, R. M. Watt, M. Kotaka, J. A. Tanner, *Proc. Mont. Acad. Sci.* **2013**, *110*, 15967–15972.
[59] S. A. Maier, *Plasmonics: Fundamentals and Applications*, Springer US, New York, NY **2007**.
[60] M. Couture, Y. Liang, H.-P. Poirier Richard, R. Faid, W. Peng, J.-F. Masson, *Nanoscale* **2013**, *5*, 12399.
[61] R. L. Olmon, B. Slovick, T. W. Johnson, D. Shelton, S. H. Oh, G. D. Boreman, M. B. Raschke, *Phys. Rev. B* **2012**, *86*, 1–9.
[62] J. Braun, B. Gompf, G. Kobiela, M. Dressel, *Phys. Rev. Lett.* **2009**, *103*, 203901.
[63] E. Kamenetskii, A. Sadreev, A. Miroshnichenko, Eds., *Fano Resonances in Optics and Microwaves*, Springer International Publishing, Cham **2018**.
[64] T. J. J. Hondrich, B. Lenyk, P. Shokoohimehr, D. Kireev, V. Maybeck, D. Mayer, A. Offenhäusser, *ACS Appl. Mater. Interfaces* **2019**, *11*, 46451–46461.
[65] N. C. Bell, C. Minelli, A. G. Shard, *Anal. Methods* **2013**, *5*, 4591–4601.
[66] A. Minopoli, N. Sakač, B. Lenyk, R. Campanile, D. Mayer, A. Offenhäusser, R. Velotta, B. Della Ventura, *Sens. Actuators B* **2020**, *308*, 127699.
[67] D. A. Armbruster, T. Pry, *Clin. Biochem. Rev.* **2008**, *29 Suppl 1*, S49–52.
[68] N. Ayawei, A. N. Ebelegi, D. Wankasi, *J. Chem.* **2017**, *2017*, 1–11.
[69] B. L. Garrote, A. Santos, P. R. Bueno, *ACS Sens.* **2019**, *4*, 2216–2227.
[70] V. Schöps, B. Lenyk, T. Huhn, J. Boneberg, E. Scheer, A. Offenhäusser, D. Mayer, *Phys. Chem. Chem. Phys.* **2018**, *20*, 4340–4346.

Manuscript received: September 15, 2020
Revised manuscript received: October 23, 2020
Accepted manuscript online: October 26, 2020